CrystEngComm

Evaluating Solvothermal and Mechanochemical Routes towards the Metal–Organic Framework Mg_2(*m*-dobdc)

Journal:	*CrystEngComm*
Manuscript ID	CE-ART-05-2022-000739.R1
Article Type:	Paper
Date Submitted by the Author:	29-Jun-2022
Complete List of Authors:	Chen, Elena; Cornell University College of Arts and Sciences, Chemistry and Chemical Biology Mandel, Ruth; Cornell University, Chemistry & Chemical Biology Milner, Phillip; Cornell University College of Arts and Sciences, Chemistry and Chemical Biology

ARTICLE

Evaluating Solvothermal and Mechanochemical Routes towards the Metal–Organic Framework Mg_2(*m*-dobdc)

Received 00th January 20xx,
Accepted 00th January 20xx

DOI: 10.1039/x0xx00000x

Elena Y. Chen,[a,†] Ruth M. Mandel,[a,†] Phillip J. Milner[a,*]

Metal–organic frameworks bearing coordinatively unsaturated Mg(II) sites are promising materials for gas storage, chemical separations, and drug delivery due to their low molecular weights and lack of toxicity. However, there remains a limited number of such MOFs reported in the literature. Herein, we investigate the gas sorption properties of the understudied framework Mg_2(*m*-dobdc) (dobdc^{4-} = 4,6-dioxido-1,3-benzenedicarboxylate) synthesized under both solvothermal and mechanochemical conditions. Both materials are found to be permanently porous, as confirmed by 77 K N_2 adsorption measurements. In particular, Mg_2(*m*-dobdc) synthesized under mechanochemical conditions using exogenous organic base displays one of the highest capacities reported to date (6.14 mmol/g) for CO_2 capture in a porous solid under simulated coal flue gas conditions (150 mbar, 40 °C). As such, mechanochemically synthesized Mg_2(*m*-dobdc) represents a promising new framework for applications requiring high gas adsorption capacities in a porous solid.

Introduction

Metal–organic frameworks (MOFs) are porous, crystalline extended solids that consist of inorganic metal nodes or secondary building units (SBUs) bridged by polytopic organic linkers.[1] Their uniquely modular structures coupled with high internal surface areas have enabled numerous applications in drug delivery, catalysis, chemical separations, and gas storage.[2–5] Frameworks containing coordinatively unsaturated metal centers, also known as open-metal site MOFs, have been extensively studied due to their ability to strongly interact with guest molecules.[6] In particular, the canonical M_2(dobdc) (M = Mg, Mn, Fe, Co, Ni, Cu, Zn, Cd; dobdc^{4-} = 2,5-dioxidobenzene-1,4-dicarboxylate), MOF-74, or CPO-27 family of frameworks features hexagonal one-dimensional channels decorated with a high density of exposed M(II) centers (Figure 1, left).[7] Among the reported isostructural metal variants, the Mg analogue, Mg_2(dobdc), is particularly promising due to its low cost, lack of toxicity, and high gravimetric and volumetric adsorption capacities for a range of adsorbates.[8–12] As such, the identification of new porous frameworks bearing accessible Mg(II) sites is highly desirable.

A closely related family of frameworks, M_2(*m*-dobdc) (M = Mg, Mn, Fe, Co, Ni; *m*-dobdc^{4-} = 4,6-dioxido-1,3-benzenedicarboxylate), have been reported to possess an even higher density of exposed cationic sites than MOF-74 materials due to slight differences in the ligand field around the metal center.[13] However, Mg_2(*m*-dobdc) prepared under solvothermal conditions was initially reported to be non-porous due to difficulties associated with removing coordinating solvents such as *N*,*N*-dimethylformamide (DMF) or methanol (MeOH) from the framework pores.[13] Although Mg_2(*m*-dobdc) was later reported to be porous when prepared under mechanochemical conditions,[14] much about its intrinsic gas sorption properties, such as the accessibility of the Mg(II) sites to guest molecules,[8] remains relatively unknown.

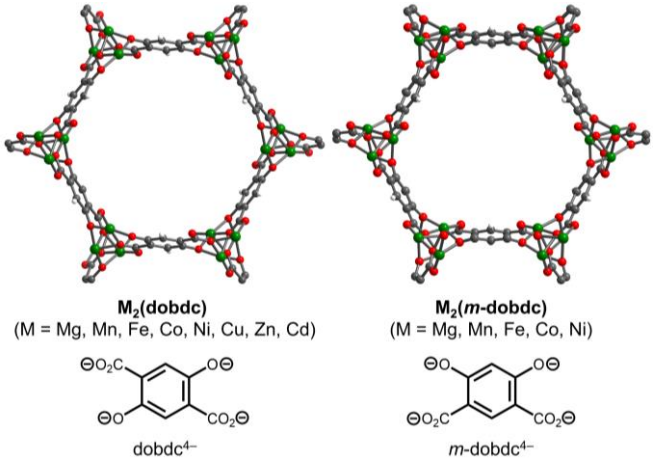

Figure 1. Structures of M_2(dobdc) (M = Mg, Mn, Fe, Co, Ni, Cu, Zn; dobdc^{4-} = 2,5-dioxidobenzene-1,4-dicarboxylate, left) and M_2(*m*-dobdc) (M = Mg, Mn, Fe, Co, Ni; *m*-dobdc^{4-} = 4,6-dioxido-1,3-benzenedicarboxylate, right). Green, gray, white, and red spheres correspond to magnesium, carbon, hydrogen, and oxygen, respectively.

Herein, we systematically investigate the synthesis and gas sorption properties of fully desolvated Mg_2(*m*-dobdc). Careful washing and activation of Mg_2(*m*-dobdc) prepared under traditional solvothermal (ST) conditions, termed Mg_2(*m*-dobdc)-ST, enables access to a material with a similar 77 K N_2 Brunauer-Emmett-Teller (BET) surface area as closely related Mg_2(dobdc). In addition, we report an improved

[a] *Department of Chemistry and Chemical Biology, Cornell University, Ithaca, NY 14850, United States*
† Contributed equally.
Electronic Supplementary Information (ESI) available: all procedures and characterization data. See DOI: 10.1039/x0xx00000x

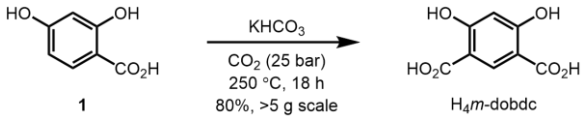

Figure 2. Synthesis of H_4*m*-dobdc from **1**.

mechanochemical (MC) method to reliably prepare Mg_2(*m*-dobdc)-MC using exogenous organic base.[14] Beyond the inherent advantages in scalability and waste minimization offered by mechanochemical syntheses,[15–17] Mg_2(*m*-dobdc)-MC exhibits higher gas adsorption capacities than Mg_2(*m*-dobdc)-ST. Indeed, at 150 mbar of CO_2 and 40 °C, conditions relevant to CO_2 capture from coal flue gas,[18] Mg_2(*m*-dobdc)-MC exhibits an higher CO_2 uptake (6.14 mmol/g) than even Mg_2(dobdc) (5.28 mmol/g).[12,19] This represents one of the highest capacities reported to date for CO_2 capture in a porous solid under simulated coal flue gas conditions.[20] Overall, our findings suggest that Mg_2(*m*-dobdc) prepared under mechanochemical conditions represents a promising and scalable alternative to ubiquitous Mg_2(dobdc) for applications in chemical separations, gas storage, and beyond.

Results and Discussion

We commenced our studies into the synthesis and gas sorption properties of Mg_2(*m*-dobdc) by optimizing the synthesis of H_4*m*-dobdc (Figure 2). In our hands, the previously reported synthesis of H_4*m*-dobdc from resorcinol via the Kolbe-Schmitt reaction was only modestly reproducible, often yielding the monocarboxylic acid **1** instead of H_4*m*-dobdc (Figure 2). Two modifications to the standard preparation were identified to make the synthesis of H_4*m*-dobdc more reliable (see Supporting Information or SI Section 2 for details). First, starting from commercially available **1** in place of resorcinol improved the reproducibility of the reaction, likely because only a single carboxylation reaction must take place to yield H_4*m*-dobdc.[21] Second, the reaction temperature (250 °C) was found to be a critical parameter and best monitored using an internal thermocouple placed directly in the solvent-free reaction mixture. With these modifications in place, we were able to reliably synthesize H_4*m*-dobdc on >5 g scale in a single batch.

The previously reported small-scale solvothermal synthesis of Mg_2(*m*-dobdc) employed $Mg_2(NO_3)_2{\cdot}6H_2O$ as the Mg precursor in 2:1 DMF:MeOH at 120 °C.[13] In order to identify the optimal solvothermal conditions for preparing Mg_2(*m*-dobdc), several combinations of amide (DMF or *N,N*-dimethylacetamide) and alcohol (MeOH, ethanol, H_2O) solvents were evaluated (SI Table S1, see SI Section 3 for details). Other methods previously reported for the preparation of Mg_2(dobdc), such as employing $Mg(OAc)_2{\cdot}4H_2O$ as a basic Mg precursor, were tested as well.[22–24] Characterization of the produced solids by powder X-ray diffraction (PXRD)[25] validated that combining H_4*m*-dobdc and $Mg_2(NO_3)_2{\cdot}6H_2O$ in 1:1 DMF:MeOH (0.03 M) at 120 °C for 48 h was optimal to yield highly crystalline Mg_2(*m*-dobdc)-ST (Figure 3, SI Figure S4). This synthesis can be readily scaled to produce Mg_2(*m*-dobdc)-ST on at least 0.5 g scale (Figure 3, SI Figure S4) and is reproducible as well (SI Figure S15). Soaking the resulting MOF in DMF at 120 °C

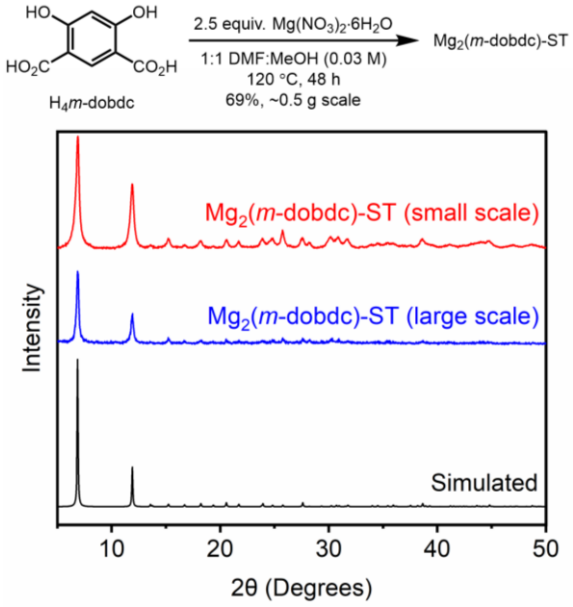

Figure 3. PXRD (λ = 1.5406 Å) patterns of Mg_2(*m*-dobdc)-ST synthesized on small and large scale under solvothermal conditions. The simulated pattern based on the previously reported single-crystal X-ray diffraction structure of the isostructural framework Co_2(*m*-dobdc) is included for reference.[25]

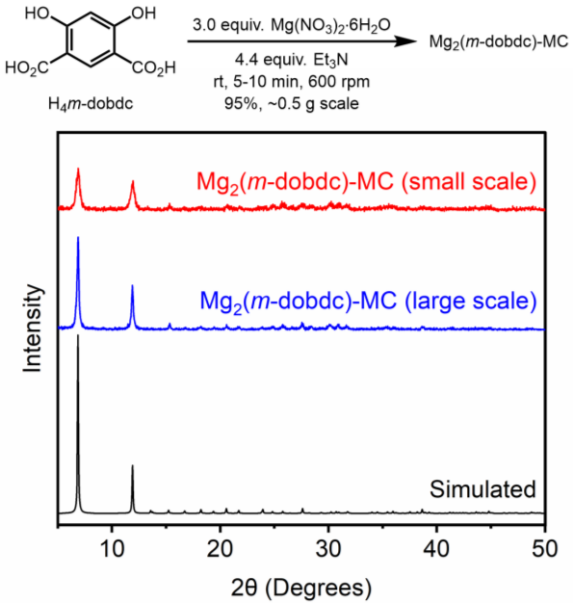

Figure 4. PXRD (λ = 1.5406 Å) patterns of Mg_2(*m*-dobdc)-MC synthesized on small and large scale under mechanochemical conditions. The simulated pattern based on the previously reported single-crystal X-ray diffraction structure of the isostructural framework Co_2(*m*-dobdc) is included for reference.[25]

to remove residual starting materials, then in MeOH at 60 °C to remove DMF, and then in acetone at room temperature to remove MeOH, was sufficient to remove coordinating solvents and soluble impurities from Mg_2(*m*-dobdc)-ST, as confirmed by acid digestion and analysis of the resulting solution by ^{1}H NMR (SI Figure S11). Unfortunately, higher reaction concentrations (>0.1 M) led to impure materials (not shown), limiting the scalability of this solvothermal method.[26]

Having optimized the solvothermal synthesis of Mg_2(*m*-dobdc), we set out to improve the mechanochemical synthesis of this material for comparison. Previously, we reported the

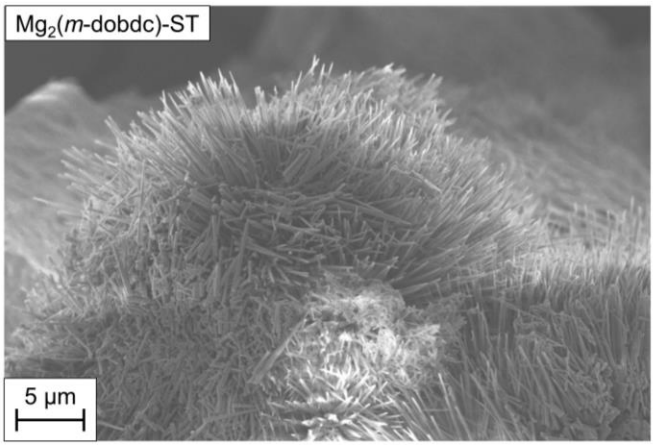

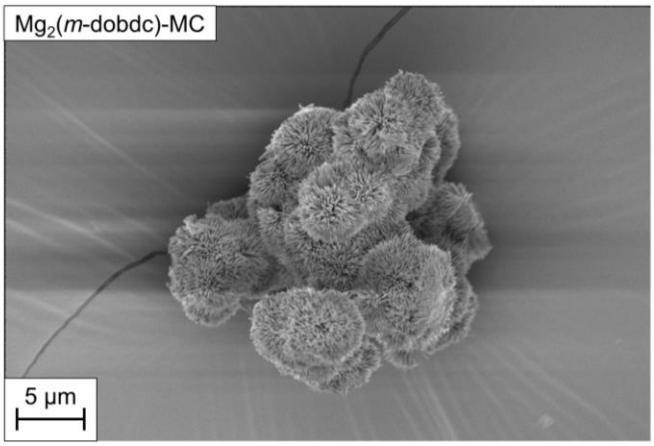

Figure 5. SEM images of Mg_2(*m*-dobdc)-ST (left) and Mg_2(*m*-dobdc)-MC (right).

Table 1. 77 K N_2 BET and Langmuir surface areas of Mg_2(*m*-dobdc)-ST and Mg_2(*m*-dobdc)-MC. Literature values reported for related Mg_2(dobdc) are included for comparison.

Material	BET Surface Area (m^2/g)	Langmuir Surface Area (m^2/g)
Mg_2(*m*-dobdc)-ST	1556 ± 2	1971 ± 3
Mg_2(*m*-dobdc)-MC	1653 ± 2	1964 ± 38
Mg_2(dobdc)	1495[12]	1905–1957[10,12]

mechanochemical synthesis of Mg_2(dobdc) using *N*,*N*-diisopropylethylamine (Hünig's base) as both the base required to deprotonate the linker precursor and as the liquid to facilitate liquid-assisted grinding in a planetary ball mill.[14] This method could be generalized to the synthesis of porous Mg_2(*m*-dobdc) with modest crystallinity. We hypothesized that careful optimization of the Mg precursor ($Mg_2(NO_3)_2{\cdot}6H_2O$, $Mg(OAc)_2{\cdot}4H_2O$, or MgO), base (Hünig's base, Et_3N, or 2,6-lutidine), and grinding time (1, 5, or 10 min) would enable the synthesis of Mg_2(*m*-dobdc)-MC with maximum crystallinity and porosity (see SI Section 4 for details). Indeed, the combination of $Mg_2(NO_3)_2{\cdot}6H_2O$, Et_3N, and 5–10 min grinding time was optimal to yield crystalline Mg_2(*m*-dobdc)-MC (Figure 4, SI Figures S16–17). This method could be reproducibly carried out with 10 min of grinding at 600 rpm to produce Mg_2(*m*-dobdc)-MC on 0.5 g scale in excellent yield (Figure 3, SI Figures S18, S28). Notably, this mechanochemical synthesis bypasses the use of toxic DMF,[27] representing a green alternative to the solvothermal synthesis of Mg_2(*m*-dobdc)-ST. No MOF was obtained with 2,6-lutidine, likely because it is not basic enough to fully deprotonate H_4(*m*-dobdc).

With optimized samples of Mg_2(*m*-dobdc)-ST and Mg_2(*m*-dobdc)-MC in hand, we compared their crystallite morphologies (Figure 5) and porosities (Table 1) in order to understand how synthesis procedure affects the physical properties of Mg_2(*m*-dobdc). Characterization of Mg_2(*m*-dobdc)-ST by scanning electron microscopy (SEM) revealed that it is composed of crystalline needles >5 µm in length on average (Figure 5 left, SI Figure S10). A needle-like morphology for Mg_2(*m*-dobdc)-ST is consistent with that previously reported for single crystals of the isostructural framework Co_2(*m*-dobdc).[25,28] Similarly, Mg_2(*m*-dobdc)-MC is comprised of needles <1 µm in length (Figure 5, right). The smaller crystallites for mechanochemically synthesized Mg_2(*m*-dobdc)-MC likely arise due to rapid deprotonation of H_4*m*-dobdc by triethylamine during the reaction.[14,29]

Careful activation of Mg_2(*m*-dobdc)-ST and Mg_2(*m*-dobdc)-MC under high vacuum (<10 µbar) at 180 °C for at least 24 h was sufficient to fully remove solvent molecules from both frameworks. Their porosities were assessed by collecting 77 K N_2 adsorption isotherms (SI Figures S7, S21). As expected, Mg_2(*m*-dobdc)-ST and Mg_2(*m*-dobdc)-MC are both microporous, with BET and Langmuir surface areas comparable to those reported for related Mg_2(dobdc) (Table 1).[10,12] The BET surface area of Mg_2(*m*-dobdc)-MC (1653 ± 2 m^2/g) is somewhat higher than that of Mg_2(*m*-dobdc)-ST (1556 ± 2), reflecting a greater degree of accessible pores and/or the presence of insoluble, amorphous impurities in the latter material. We note that heating Mg_2(*m*-dobdc) with ramp rates faster than 1 °C/min or to temperatures greater than 180 °C consistently led to lower surface areas, likely due to partial pore collapse. Nonetheless, these findings confirm that highly porous and crystalline Mg_2(*m*-dobdc) can be readily prepared under both solvothermal and mechanochemical conditions.

Given the microporosity of both Mg_2(*m*-dobdc) samples and the high capacities of closely related Mg_2(dobdc) for a range of adsorbates,[10,12] we assessed the potential suitability of Mg_2(*m*-dobdc)-ST and Mg_2(*m*-dobdc)-MC for gas capture applications using CO_2 scrubbing from coal flue gas as a representative separation. As such, CO_2 adsorption and desorption isotherms at 30 °C, 40 °C, and 50 °C and N_2 adsorption and desorption isotherms at 40 °C were collected for Mg_2(*m*-dobdc)-ST (Figure 6a, SI Figures S12–13) and Mg_2(*m*-dobdc)-MC (Figure 6b, SI Figures S25–26). In all cases, gas sorption was found to be completely reversible. Both materials exhibit steep uptake at low CO_2 pressures, indicative of strong interaction of CO_2 with exposed Mg(II) sites.[12] The maximum CO_2 uptake for both materials at 30 °C and 1 bar of CO_2 are 6.50 mmol/g for Mg_2(*m*-dobdc)-ST and 8.69 mmol/g for Mg_2(*m*-dobdc)-MC; the latter value is similar to that predicted for binding one CO_2 per Mg(II) site in this material (8.24 mmol/g). The higher CO_2 capacity of Mg_2(*m*-dobdc)-MC than Mg_2(*m*-dobdc)-ST is consistent with its higher 77 K N_2 BET surface area and suggests that the

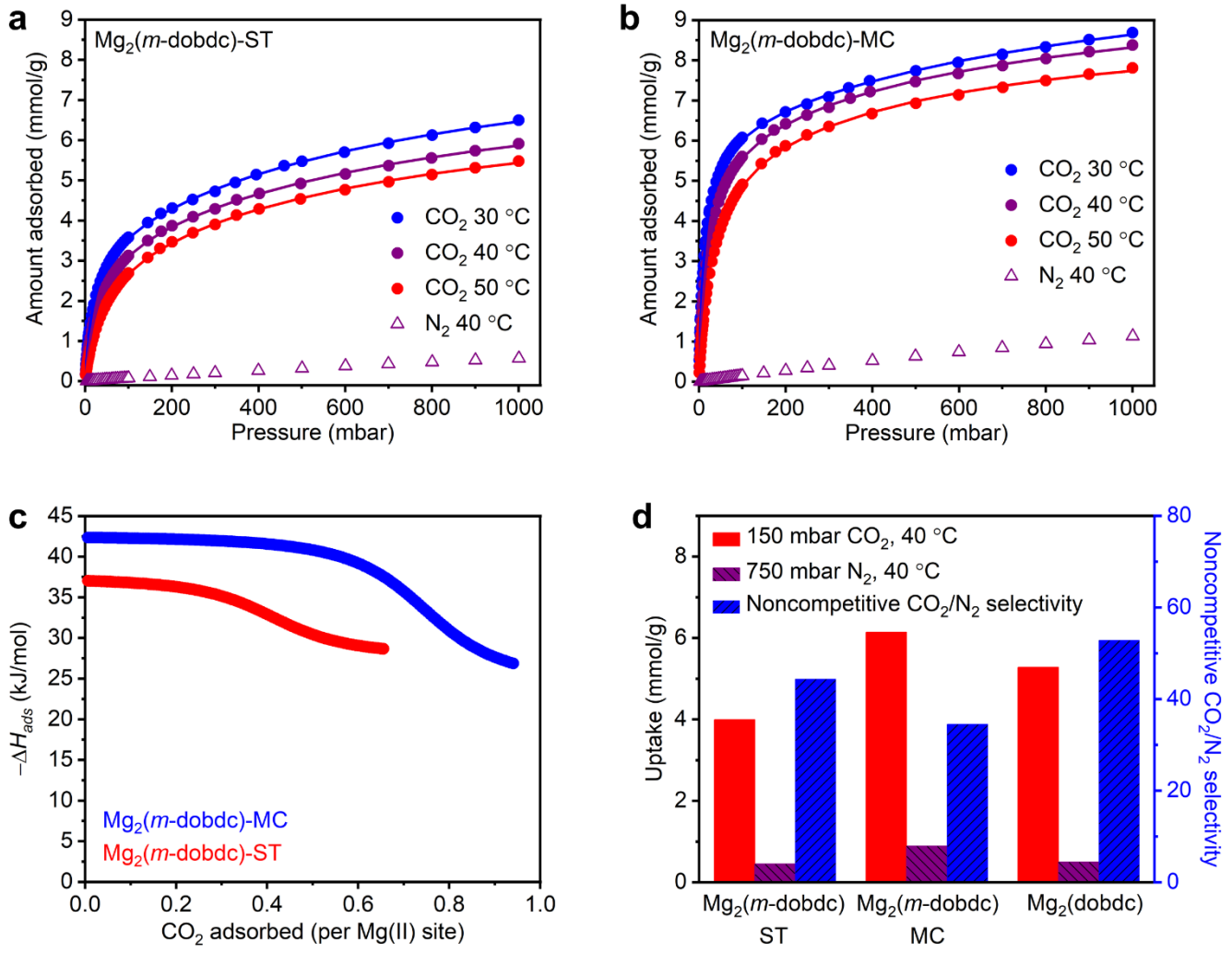

Figure 6. 30 °C, 40 °C, and 50 °C CO_2 and 40 °C N_2 adsorption isotherms in a) Mg_2(*m*-dobdc)-ST and b) Mg_2(*m*-dobdc)-MC. The lines correspond to individual fits to the dual-site Langmuir model. A data point was considered equilibrated when <0.01% pressure change occurred over a 30 s interval. c) Enthalpy of adsorption ($-\Delta H_{ads}$) values for Mg_2(*m*-dobdc)-ST and Mg_2(*m*-dobdc)-MC determined using simultaneous fits to dual-site Langmuir models. d) Summary of CO_2 and N_2 uptake values and non-competitive CO_2/N_2 selectivities relevant to CO_2 capture from coal flue gas for Mg_2(*m*-dobdc)-ST and Mg_2(*m*-dobdc)-MC. The corresponding values for Mg_2(dobdc) reported in the literature are included for reference.[19]

mechanochemically synthesized MOF has more accessible Mg(II) sites.

To confirm that CO_2 binding in Mg_2(*m*-dobdc) materials likely occurs at coordinatively unsaturated Mg(II) sites, the CO_2 adsorption isotherms were fit using dual-site Langmuir models both independently and simultaneously (SI Tables S2, S4). The independent dual-site Langmuir model fits are included in Figure 6a-b and represent good fits to the experimental data. Using the Clausius-Clapeyron relationship, the differential enthalpies of adsorption ($-\Delta H_{ads}$) as a function of CO_2 loading were calculated (Figure 6c, SI Figures S14, S27). The $-\Delta H_{ads}$ values at low coverage are comparable for Mg_2(*m*-dobdc)-MC (42 kJ/mol) and Mg_2(*m*-dobdc)-ST (37 kJ/mol) and are similar to those previously reported for CO_2 adsorption in MOFs bearing accessible Mg(II) sites as well (38–43 kJ/mol).[10,30] The $-\Delta H_{ads}$ plots support that Mg_2(*m*-dobdc)-MC contains more accessible Mg(II) sites than Mg_2(*m*-dobdc)-ST, as the strong binding of CO_2 drop offs at higher loadings in this material (~0.7 CO_2 per Mg vs. ~0.4 CO_2 per Mg in Mg_2(*m*-dobdc)-ST).

Among MOFs, Mg_2(dobdc) possesses one of the highest reported CO_2 capacities (5.28 mmol/g) under conditions relevant to CO_2 capture from coal flue gas (150 mbar, 40 °C) (Figure 6d).[10,18,19] Coupled with minimal uptake of N_2 at 750 mbar and 40 °C (0.50 mmol/g),[19] this high CO_2 uptake at low pressures makes Mg_2(dobdc) a promising material for CO_2/N_2 separations. While the CO_2 uptake of Mg_2(*m*-dobdc)-ST at 150 mbar and 40 C (3.99 mmol/g) is less than that reported for Mg_2(dobdc), likely due to its dearth of accessible Mg(II) sites, Mg_2(*m*-dobdc)-MC exhibits a higher capacity for CO_2 (6.14 mmol/g) than Mg_2(dobdc) under these conditions (Figure 6d). Previous studies have suggested that the metal centers of M_2(*m*-dobdc) MOFs are slightly more Lewis acidic than those of M_2(dobdc) MOFs,[13] which may account for the enhanced CO_2 uptake at low pressures in Mg_2(*m*-dobdc)-MC. Consistently, the N_2 capacity of Mg_2(*m*-dobdc)-MC at 750 mbar and 40 °C (0.89 mmol/g) is higher than that reported for Mg_2(dobdc) as well. Given the unclear suitability of calculating selectivities in open metal site MOFs using ideal adsorbed solution theory (IAST),[31] we elected to calculate non-competitive CO_2/N_2 selectivities

under conditions relevant to coal flue gas capture for Mg_2(*m*-dobdc)-ST, Mg_2(*m*-dobdc)-MC, and Mg_2(dobdc) instead (Figure 6d). The non-competitive CO_2/N_2 selectivity calculated for Mg_2(dobdc) is the highest (53),[19] followed by Mg_2(*m*-dobdc)-ST (44), and then Mg_2(*m*-dobdc)-MC (35). The diminished non-competitive CO_2/N_2 selectivity for Mg_2(*m*-dobdc)-MC is due to the higher uptake of N_2 in this material. Nonetheless, these findings support that Mg_2(*m*-dobdc)-MC is competitive with the widely studied MOF Mg_2(dobdc) for this representative separation. Further, the superior gas sorption performance of Mg_2(*m*-dobdc)-MC over Mg_2(*m*-dobdc)-ST indicates that mechanochemical methods may be preferable for the scalable synthesis of this framework.

Conclusions

Owing to their low cost and high gravimetric gas storage capacities, MOFs bearing high densities of coordinatively unsaturated Mg(II) centers are highly sought after. We have demonstrated that Mg_2(*m*-dobdc) synthesized under mechanochemical competitions is a promising new Mg-based MOF due to its strong binding and high capacity for CO_2 at low pressures. Notably, the work presented herein represents a rare example in which a mechanochemically synthesized MOF displays superior gas sorption properties compared to material synthesized under traditional solvothermal conditions.[14–17] Moving forward, mechanochemical methods will prove to be a valuable alternative to solvothermal syntheses for the preparation of high-quality MOFs for applications in gas storage, chemical separations, and drug delivery.

Acknowledgements

The development of new methods for the synthesis of Mg-based MOFs was supported by the National Institute of General Medical Sciences of the National Institutes of Health under award number R35GM138165. The content is solely the responsibility of the authors and does not necessarily represent the official views of the National Institutes of Health. The characterization of the CO_2 adsorption properties of Mg_2(*m*-dobdc) was supported by the U.S. Department of Energy, Office of Science, Office of Basic Energy Sciences under Award Number DE-SC0021000. This work made use of the Cornell Center for Materials Research Shared Facilities, which are supported through the NSF MRSEC program (DMR-1719875). Some of the ^{1}H NMR data in this work were collected on a Bruker INOVA 500 MHz spectrometer that was purchased with support from the NSF (CHE-1531632). We thank Cornell University for providing a Summer Experience Grant to E.Y.C.

Author Contributions

P.J.M. and R.M.M. conceived the project. E.Y.C. and R.M.M. carried out all experiments. The manuscript was written through the contributions of all authors, and all authors approved of the final version.

Conflicts of interest

P.J.M. is listed as an inventor on several patents related to the application of MOFs for gas capture.

Notes and references

1 H. Furukawa, K. E. Cordova, M. O'Keeffe and O. M. Yaghi, *Science*, 2013, **341**, 1230444.
2 Y. Sun, L. Zheng, Y. Yang, X. Qian, T. Fu, X. Li, Z. Yang, H. Yan, C. Cui and W. Tan, *Nano-Micro Lett.*, 2020, **12**, 103.
3 A. Bavykina, N. Kolobov, I. S. Khan, J. A. Bau, A. Ramirez and J. Gascon, *Chem. Rev.*, 2020, **120**, 8468–8535.
4 H. Li, K. Wang, Y. Sun, C. T. Lollar, J. Li and H.-C. Zhou, *Materials Today*, 2018, **21**, 108–121.
5 C. A. Trickett, A. Helal, B. A. Al-Maythalony, Z. H. Yamani, K. E. Cordova and O. M. Yaghi, *Nat. Rev. Mater.*, 2017, **2**, 17045.
6 Ü. Kökçam-Demir, A. Goldman, L. Esrafili, M. Gharib, A. Morsali, O. Weingart and C. Janiak, *Chem. Soc. Rev.*, 2020, **49**, 2751–2798.
7 N. L. Rosi, J. Kim, M. Eddaoudi, B. Chen, M. O'Keeffe and O. M. Yaghi, *J. Am. Chem. Soc.*, 2005, **127**, 1504–1518.
8 M. E. Zick, J.-H. Lee, M. I. Gonzalez, E. O. Velasquez, A. A. Uliana, J. Kim, J. R. Long and P. J. Milner, *J. Am. Chem. Soc.*, 2021, **143**, 1948–1958.
9 À. Ruyra, A. Yazdi, J. Espín, A. Carné-Sánchez, N. Roher, J. Lorenzo, I. Imaz and D. Maspoch, *Chem. Eur. J.*, 2015, **21**, 2508–2518.
10 W. L. Queen, M. R. Hudson, E. D. Bloch, J. A. Mason, M. I. Gonzalez, J. S. Lee, D. Gygi, J. D. Howe, K. Lee and T. A. Darwish, *Chem. Sci.*, 2014, **5**, 4569–4581.
11 T. Grant Glover, G. W. Peterson, B. J. Schindler, D. Britt and O. Yaghi, *Chem. Eng. Sci.*, 2011, **66**, 163–170.
12 S. R. Caskey, A. G. Wong-Foy and A. J. Matzger, *J. Am. Chem. Soc.*, 2008, **130**, 10870–10871.
13 M. T. Kapelewski, S. J. Geier, M. R. Hudson, D. Stück, J. A. Mason, J. N. Nelson, D. J. Xiao, Z. Hulvey, E. Gilmour, S. A. FitzGerald, M. Head-Gordon, C. M. Brown and J. R. Long, *J. Am. Chem. Soc.*, 2014, **136**, 12119–12129.
14 Z. Wang, Z. Li, M. Ng and P. J. Milner, *Dalton Trans.*, 2020, **49**, 16238–16244.
15 D. Chen, J. Zhao, P. Zhang and S. Dai, *Polyhedron*, 2019, **162**, 59–64.
16 J. L. Howard, Q. Cao and D. L. Browne, *Chem. Sci.*, 2018, **9**, 3080–3094.
17 T. Friščić, in *Encyclopedia of Inorganic and Bioinorganic Chemistry*, John Wiley & Sons, Ltd, 2014, pp. 1–19.
18 E. J. Granite and H. W. Pennline, *Ind. Eng. Chem. Res.*, 2002, **41**, 5470–5476.
19 J. A. Mason, K. Sumida, Z. R. Herm, R. Krishna and Jeffrey. R. Long, *Energy Environ. Sci.*, 2011, **4**, 3030.
20 A. Modak and S. Jana, *Microporous Mesoporous Mater.* 2019, **276**, 107–132.
21 Y. Sadamitsu, A. Okumura, K. Saito and T. Yamada, *Chem. Commun.*, 2019, **55**, 9837–9840.
22 K. A. Colwell, M. N. Jackson, R. M. Torres-Gavosto, S. Jawahery, B. Vlaisavljevich, J. M. Falkowski, B. Smit, S. C. Weston and J. R. Long, *J. Am. Chem. Soc.*, 2021, **143**, 5044–5052.
23 L. Garzón-Tovar, A. Carné-Sánchez, C. Carbonell, I. Imaz and D. Maspoch, *J. Mat. Chem. A*, 2015, **3**, 20819–20826.
24 D. J. Tranchemontagne, J. R. Hunt and O. M. Yaghi, *Tetrahedron*, 2008, **64**, 8553–8557.
25 J. E. Bachman, M. T. Kapelewski, D. A. Reed, M. I. Gonzalez and J. R. Long, *J. Am. Chem. Soc.*, 2017, **139**, 15363–15370.

26 D. R. Du Bois, K. R. Wright, M. K. Bellas, N. Wiesner and A. J. Matzger, *Inorg. Chem.*, 2022, **61**, 4550–4554.
27 F. P. Byrne, S. Jin, G. Paggiola, T. H. M. Petchey, J. H. Clark, T. J. Farmer, A. J. Hunt, C. Robert McElroy and J. Sherwood, *Sustain. Chem. Process*, 2016, **4**, 7.
28 M. I. Gonzalez, M. T. Kapelewski, E. D. Bloch, P. J. Milner, D. A. Reed, M. R. Hudson, J. A. Mason, G. Barin, C. M. Brown and J. R. Long, *J. Am. Chem. Soc.*, 2018, **140**, 3412–3422.
29 G. Ayoub, B. Karadeniz, A. J. Howarth, O. K. Farha, I. Đilović, L. S. Germann, R. E. Dinnebier, K. Užarević and T. Friščić, *Chem. Mater.*, 2019, **31**, 5494–5501.
30 P. J. Milner, J. D. Martell, R. L. Siegelman, D. Gygi, S. C. Weston and J. R. Long, *Chem. Sci.*, 2018, **9**, 160–174.
31 R. Krishna and J. M. van Baten, *ACS Omega*, 2021, **6**, 15499–15513.